This article was downloaded by: [Institute Of Atmospheric Physics]
On: 09 December 2014, At: 15:25
Publisher: Taylor & Francis
Informa Ltd Registered in England and Wales Registered Number: 1072954 Registered office: Mortimer House, 37-41 Mortimer Street, London W1T 3JH, UK

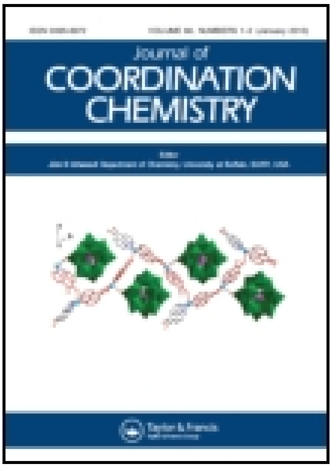

Click for updates

Journal of Coordination Chemistry
Publication details, including instructions for authors and subscription information:
http://www.tandfonline.com/loi/gcoo20

Synthesis, solution properties, and solid-state structural analysis of [Mn(κ^4-N,N,S,N-dpktsc)Br]$_2$·nCH$_3$CN (n=1 or 0 and dpktsc=di-2-pyridyl ketone thiosemicarbazone)

Mohammed Bakir[a], Rebecca Conry[b] & Donovan Thomas[a]
[a] Department of Chemistry, The University of the West Indies-Mona Campus, Kingston, Jamaica
[b] Department of Chemistry, Colby College, Waterville, ME, USA
Published online: 20 Feb 2014.

To cite this article: Mohammed Bakir, Rebecca Conry & Donovan Thomas (2014) Synthesis, solution properties, and solid-state structural analysis of [Mn(κ^4-N,N,S,N-dpktsc)Br]$_2$·nCH$_3$CN (n=1 or 0 and dpktsc=di-2-pyridyl ketone thiosemicarbazone), Journal of Coordination Chemistry, 67:2, 249-264, DOI: 10.1080/00958972.2013.865838

To link to this article: http://dx.doi.org/10.1080/00958972.2013.865838

PLEASE SCROLL DOWN FOR ARTICLE

Taylor & Francis makes every effort to ensure the accuracy of all the information (the “Content”) contained in the publications on our platform. However, Taylor & Francis, our agents, and our licensors make no representations or warranties whatsoever as to the accuracy, completeness, or suitability for any purpose of the Content. Any opinions and views expressed in this publication are the opinions and views of the authors, and are not the views of or endorsed by Taylor & Francis. The accuracy of the Content should not be relied upon and should be independently verified with primary sources of information. Taylor and Francis shall not be liable for any losses, actions, claims, proceedings, demands, costs, expenses, damages, and other liabilities whatsoever or howsoever caused arising directly or indirectly in connection with, in relation to or arising out of the use of the Content.

This article may be used for research, teaching, and private study purposes. Any substantial or systematic reproduction, redistribution, reselling, loan, sub-licensing, systematic supply, or distribution in any form to anyone is expressly forbidden. Terms &

Conditions of access and use can be found at http://www.tandfonline.com/page/terms-and-conditions

Downloaded by [Institute Of Atmospheric Physics] at 15:25 09 December 2014

Journal of Coordination Chemistry, 2014
Vol. 67, No. 2, 249–264, http://dx.doi.org/10.1080/00958972.2013.865838

Synthesis, solution properties, and solid-state structural analysis of [Mn(κ^4-N,N,S,N-dpktsc)Br]$_2$·nCH$_3$CN (n = 1 or 0 and dpktsc = di-2-pyridyl ketone thiosemicarbazone)

MOHAMMED BAKIR*†, REBECCA CONRY‡ and DONOVAN THOMAS†

†Department of Chemistry, The University of the West Indies-Mona Campus, Kingston, Jamaica
‡Department of Chemistry, Colby College, Waterville, ME, USA

(*Received 15 August 2013; accepted 31 October 2013*)

Downloaded by [Institute Of Atmospheric Physics] at 15:25 09 December 2014

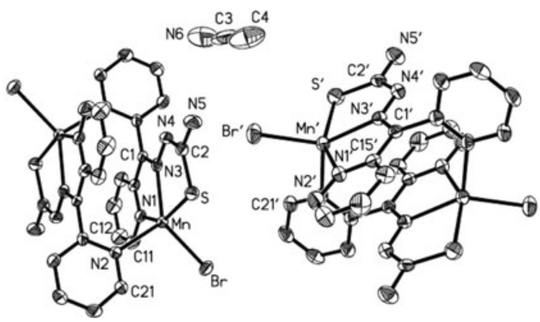

Ultrasonic radiation of a mixture of [Mn(CO)$_5$Br], [dpktsc], and CH$_3$CN gave [Mn(κ^4-N,N,S,N-dpktsc)Br]$_2$·nCH$_3$CN (n = 0 or 1). Under reflux, a mixture of [Mn(CO)$_5$Br], [dpktsc], and CH$_3$CN gave [Mn(κ^3-N,N,S-dpktsc-H)$_2$]·2H$_2$O. Crystals of [Mn(κ^4-N,N,S,N-dpktsc)Br]$_2$ were obtained by the evaporation of CH$_3$CN from crystals of [Mn(κ^4-N,N,S,N-dpktsc)Br]$_2$·CH$_3$CN. The solid-state structures of [Mn(κ^4-N,N,S,N-dpktsc)Br]$_2$·nCH$_3$CN (n = 0 or 1) reveal two independent centrosymmetric dimers in the unit cell of each crystal and one CH$_3$CN in the case of solvated crystal. Crystals of [Mn(κ^4-N,N,S,N-dpktsc)Br]$_2$·nCH$_3$CN are stabilized by a network of non-covalent interactions that include hydrogen bonds and π–π interactions. Spectroscopic measurements reveal sensitivity of protophilic solutions of [Mn(κ^4-N,N,S,N-dpktsc)Br]$_2$ and [Mn(κ^3-N,N,S-dpktsc-H)$_2$]·2H$_2$O to changes in their surroundings, as manifested by changes in the intensity of electronic absorption spectral properties in the presence and absence of external stimulus (acid or base). Electrochemical measurements in DMF reveal two closely spaced reduction/oxidation couples due to Mn^I → Mn^0 and Mn^I → Mn^{II} of the dimer. In the case of [Mn(κ^3-N,N,S-dpktsc-H)$_2$]·2H$_2$O, two well-separated reductions appeared due to Mn^{II} → Mn^I and Mn^I → Mn^0. Electrochemical reactions of [Mn(κ^4-N,N,S,N-dpktsc)Br]$_2$ and [Mn(κ^3-N,N,S-dpktsc-H)$_2$]·2H$_2$O show the monomer to be more active toward CO$_2$ than the dimer.

Keywords: Di-2-pyridyl ketone thiosemicarbazone; Manganese; Spectroscopy; X-ray; Electrochemistry

*Corresponding author. Email: mohammed.bakir@uwimona.edu.jm

© 2014 Taylor & Francis

1. Introduction

Thiosemicarbazones [$R^1R^2C{=}N{-}NH{-}CS{-}NR^3R^4$ where R^1 or R^2 = alkyl or aryl groups and R^3 and R^4 = hydrogen, alkyl, or aryl)] and their metal complexes continue to attract research activities because of their physical properties, reactivity patterns, and applications in several chemical and biological processes [1–20]. Thiosemicarbazones possess a wide range of biological activities that include anticancer, antibacterial, antifungal, antiviral, etc. and several derivatives are in use as diagnostic and therapeutic agents [1–5]. The therapeutic properties of thiosemicarbazones are partly due to their ability to chelate to metal ions, thus depriving cells from essential nutrients and leading to cell death [1, 4]. Many catalytic processes such as Suzuki–Miyaura cross-couplings, oxidation, hydrogenation, olefin cyclopropanations, etc. utilize thiosemicarbazone derivatives [6–9]. Thiosemicarbazones are widely used as sensitive analytical reagents for detection and determination of trace metals in environmental, pharmaceutical, and biological samples, and in the extraction of metals for the inhibition of corrosion, etc. [10–13]. Despite immense efforts devoted to develop chemotherapeutics, catalytic, and analytical agents based on thiosemicarbazones, the coordination chemistry of di-2-pyridyl ketone thiosemicarbazone, [dpktsc = $(py)_2C{=}N{-}NH{-}CS{-}NH_2$] is limited [16–21]. Both di-2-pyridyl ketone thiosemicarbazone [dpktsc] and its amide deprotonated conjugate base, $[\text{dpktsc-H}]^-$, coordinate to metal moieties in bidentate, tridentate, and quadridentate fashions to form mononuclear and binuclear complexes [16–21]. As a bidentate ligand, [dpktsc] binds either through the nitrogen atoms of the pyridine rings or one nitrogen atom of a pyridine ring and the imino nitrogen atom to form complexes of the type *fac*-$[M(CO)_3(\kappa^2\text{-N,N-dpktsc})Cl]\cdot nMeOH)$ (M = Re, $n = 0$ and M = Tc, $n = 0.5$) [20, 21]. When coordinated in the tridentate fashion, $[\text{dpktsc-H}]^-$ binds to the metal center through a nitrogen atom of a pyridine ring, the imino nitrogen atom, and the sulfur atom leaving a nitrogen atom of a pyridine ring uncoordinated to form compound of the type $[M(\kappa^3\text{-N,N,S-dpktsc-H})_2]^{0/+1}\cdot nH_2O$ (M = Zn, Fe and Mn) [16, 17]. In the quadridentate coordination mode, all potential coordinating atoms (nitrogen and sulfur) bind to form binuclear complexes such as $[Cu(\kappa^4\text{-N,N,S,N-dpktsc-H})X]_2\cdot Y$ (X = Cl or CN and Y = DMF or MeOH) and $[Re_2(CO)_6X(\kappa^4\text{-N,N,S,N-dpktsc-H})]$ (X = Cl or Br) [18, 19].

In this report, we describe the reactions of $[Mn(CO)_5Br]$ with [dpktsc] that gave dimeric manganese compounds of [dpktsc] and a mononuclear manganese compound of $[\text{dpktsc-H}]^-$. In addition, details are given for the solution chemistry of the isolated products and the solid-state structures of solvated and solvent free manganese dimers of [dpktsc]. We have been interested in the chemistry of di-2-pyridyl ketone derivatives (see scheme 1) and have

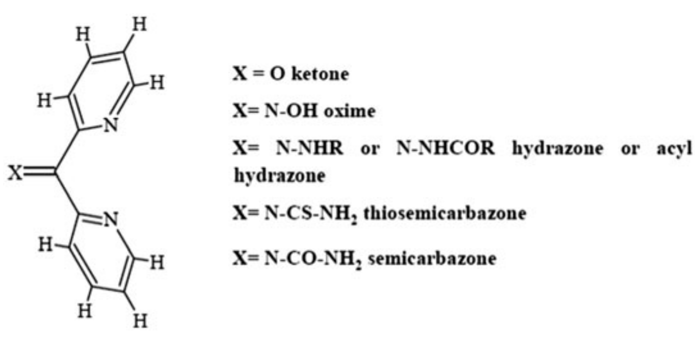

Scheme 1. Representation of selected di-2-pyridyl ketone derivatives.

Downloaded by [Institute Of Atmospheric Physics] at 15:25 09 December 2014

previously reported on the synthesis and physical properties of a series of metal compounds containing di-2-pyridyl ketone derivatives [21–26]. Our interest in the chemistry of di-2-pyridyl ketone derivatives is due to their diverse coordination modes, rich physico-chemical properties, and potential applications in several areas [27–32].

2. Experimental

2.1. *Reagents and reaction procedures*

The ligand [dpktsc], melting point 256–258 °C, was prepared by refluxing di-2-pyridyl ketone (dpk) and thiosemicarbazide in acidified EtOH as described previously [16, 22]. All other reagents were purchased from commercial sources and used without purification. Ultrasonic reactions were carried out using Branson 200 with ultrasonic energy 40 kHz.

2.2. *Synthesis of [Mn(κ^4-N,N,S,N-dpktsc)Br]$_2$·nCH$_3$CN (n = 0, 1)*

Equimolar CH_3CN solutions (10 mL each) of $Mn(CO)_5Br$ (0.30 g, 1.12 mM) and dpktsc (0.30 g, 1.10 M) were mixed and subjected to ultrasonic radiation in air for 0.5 h and left to stand at room temperature for 2 days. Purple crystals were isolated by filtration and a single crystal of [Mn(η^4-N,N,S,N-dpktsc)Br]$_2$·CH_3CN was selected and subjected to X-ray analysis before drying. The remaining crystals were allowed to dry in air; yield 0.17 g (0.22 mM, 40%). Anal. Calcd for $C_{24}H_{22}Br_2Mn_2N_{10}S_2$ (%): C, 36.75; H, 2.83; N, 17.86. Found: C, 36.32; H, 2.78; N, 18.32. Infrared (IR) data: *ν*(N–H) 3448, 3320, 3184, *ν*(C–H) 3069, *ν*(C=C) and *ν*(C=N) at 1593, 1561 and 1483, *ν*(C=S) 1225 and *ν*(N–N) 1152 cm^{-1}. ^{1}H NMR (*δ* ppm): in DMSO-d$_6$ at 303 K: 12.98 (1H, NH), 8.83 (1H, dpk), 8.74 (1H, dpk), 8.56 (1H, NH_2), 8.35 (1H, NH_2), 8.29 (1H dpk), 8.00 (1H, dpk), 7.94 (1H, dpk), 7.58 (1H, dpk), 7.52 (H dpk), 7.45 (1H, dpk) and 3.42 (dissolved water in DMSO-d$_6$). UV–vis {*λ*/nm, ($\varepsilon \pm 500$/cm^{-1} M^{-1})} CH_3CN: 388 (11,800), 320 (21,000), 272 (29,000); DMSO: 412 (52,000), 345 (37,000); DMF: 412 (55,600), 345 (27,500).

2.3. *Synthesis of [Mn(κ^3-N,N,S,-dpktsc-H)$_2$]·2H$_2$O*

A mixture of [$Mn(CO)_5Br$] (0.20 g, 0.73 mM), [dpksc] (0.45 g, 1.75 mM) and CH_3CN (50 mL) was refluxed for 4 h and allowed to cool to room temperature. An orange-yellow precipitate was filtered off, washed with hexanes, diethyl ether, and dried; yield 0.35 g (0.59 mM, 34%). Anal. Calcd for $C_{24}H_{24}MnN_{10}O_2S_2$ (%): C, 47.76; H, 4.01; N, 23.21. Found: C, 47.88; H, 3.15; N, 23.89. IR data: *ν*(N–H) 3498, 3374, 3375, 3289, *ν*(C–H) 3187, *ν*(C=C) and *ν*(C=N) at 1614, 1587 and 1481, *ν*(C=S) 1220 and *ν*(N–N) 1136 cm^{-1}. UV–vis {*λ*/nm, (*ε*/cm^{-1} M^{-1})} DMSO: 412 (25,000 ± 500); DMF: 408 (25,700 ± 500).

2.4. *Physical measurements*

A HP-8452A spectrophotometer in conjunction with Lauda-Brinkmann RM6 circulating bath was used to measure the electronic absorption spectra. Solution ^{1}H NMR spectra were recorded on a Bruker Avance 500-MHz DRX Fourier-transform spectrometer and referenced to the residual protons in the incompletely deuterated solvent. IR spectra were

Downloaded by [Institute Of Atmospheric Physics] at 15:25 09 December 2014

recorded as KBr disks on a Perkin-Elmer Spectrum 1000 FT-IR spectrometer. Electrochemical measurements were performed with the use of a Princeton Applied Research (PAR) Model 173 potentiostat/galvanostat and Model 276 interface in conjunction with a digital Celebris 466 PC. Data were acquired with the EG&G PARC Headstart program and manipulated using Microsoft Excel. Measurements were performed in solutions that were 0.1 M in N(n-Bu)PF_6. The $E_{p,a}$, $E_{p,c}$, and $E_{1/2} = (E_{p,a} + E_{p.c})/2$ values were referenced to the saturated calomel electrode (SCE) at room temperature and are uncorrected for junction potentials. Electrochemical cells were of conventional design, based on scintillation vials or H-cells. A glassy carbon disk was the working electrode and a Pt wire was the counter-electrode.

2.5. *X-ray crystallography*

Crystals of [Mn(κ^4-N,N,S,N-dpktsc)Br]$_2 \cdot n$$CH_3CN$ ($n = 0$ or 1) were obtained from the reaction mixture before and after drying. Data collection on a freshly isolated single crystal of [Mn(κ^4-N,N,S,N-dpktsc)Br]$_2 \cdot$$CH_3CN$ started on the same day the crystal was isolated from the reaction mixture while data collection on [Mn(κ^4-N,N,S,N-dpktsc)Br]$_2$ was done several days after the crystals were isolated from the reaction mixture. A single crystal of each dimer was selected and mounted on a glass fiber using epoxy cement prior to data collection. Bruker AXS and Bruker SMART CCD area-detector diffractometers with

Table 1. Crystal data and structure refinement of [Mn(κ^4-N,N,S,N-dpktsc)Br]$_2 \cdot n$$CH_3CN$ ($n = 0$ or 1).

Empirical formula	$C_{24}H_{22}Br_2Mn_2N_{10}S_2$	$C_{26}H_{25}Br_2Mn_2N_{11}S_2$
Formula weight	784.34	841.39
Temperature (K)	296(2)	297(2)
Wavelength (Å)	0.71073	0.71073
Crystal system, space group	Triclinic, *P-1*	Triclinic, *P-1*
Unit cell dimensions (Å, °)		
a	9.6614(6)	9.713(4)
b	12.0880(7)	12.510(2)
c	14.0652(8)	14.254(4)
α	82.5060(10)	84.79(2)
β	72.6210(10)	74.35(2)
γ	81.1230(10)	79.00(2)
Volume (Å^3)	1542.66(16)	1635.7(8)
Z, calculated density (Mg m^{-3})	2, 1.689	2, 1.708
Absorption coefficient (mm^{-1})	3.577	3.383
F(0 0 0)	776	836
θ Range for data collection (°)	1.52–28.27	2.27–25.00
Limiting indices	$-11 \rightarrow 12$	$-11 \rightarrow 1$
h	$-16 \rightarrow 16$	$-14 \rightarrow 14$
k	$-17 \rightarrow 18$	$-16 \rightarrow 16$
l		
Reflections collected/unique	7348/4323	6197/5185
[*R*(int)]	0.0496	0.0643
Completeness to $\theta = 28.27$	56.6%	90.1%
Absorption correction	None	Empirical
Max. and min. transmission		0.5048 and 0.3022
Refinement method	Full-matrix least-squares on F^2	
Data/restraints/parameters	4323/0/363	5185/0/390
Goodness-of-fit on F^2	0.640	1.046
Final *R* indices [$I > 2\sigma(I)$]	$R1 = 0.0507$, $wR2 = 0.1035$	$R1 = 0.0742$, $wR2 = 0.2123$
R indices (all data)	$R1 = 0.0950$, $wR2 = 0.1127$	$R1 = 0.1070$, $wR2 = 0.2415$
Largest diff. peak and hole (e Å^{-3})	0.350 and −0.244	1.048 and −1.309

Downloaded by [Institute Of Atmospheric Physics] at 15:25 09 December 2014

Mo-K_α radiation and a graphite monochromator were used for data collection of [Mn(κ^4-N,N,S,N-dpktsc)Br]$_2$·CH_3CN and [Mn(κ^4-N,N,S,N-dpktsc)Br]$_2$, respectively. The SHELXTL software package version 5.1 and PLATON software version 240413 were used for structure analysis [33–35]. Cell parameters and other crystallographic information are given in table 1. The atomic coordinates and equivalent isotropic displacement parameters are given in Supplementary material (see online supplemental material at http://dx.doi.org/10.1080/00958972.2013.865838). All non-hydrogen atoms were refined with anisotropic thermal parameters.

2.6. *Analytical procedures*

Elemental microanalyses were performed by MEDAC Ltd, Department of Chemistry, Brunel University, Uxbridge, UK.

3. Results and discussion

The ultrasonic radiation of an equimolar mixture of [Mn(CO)$_5$Br], [dpktsc] and CH_3CN gave purple crystals of [Mn(κ^4-N,N,S,N-dpktsc)Br]$_2$·$n$$CH_3CN$ ($n = 0$ or 1). Crystals of [Mn(κ^4-N,N,S,N-dpktsc)Br]$_2$ were obtained from evaporation of CH_3CN from crystals of [Mn(κ^4-N,N,S,N-dpktsc)Br]$_2$·$n$$CH_3CN$. This reaction is in contrast to the reaction of [Re(CO)$_5$Cl] with [dpktsc] in refluxing toluene that gave pyridyl-N,N-bidentate coordination of [dpktsc] to form *fac*-[Re(CO)$_3$(κ^2-N,N-dpktsc)Cl] [21]. This reaction also contrasts to the ultrasonic radiation of a mixture of [Mn(CO)$_5$Br], [dpktah] (dpktah = di-2-pyridyl ketone thiophenecarboxylic acid hydrazone) and diethyl ether that gave *fac*-[Mn(CO)$_3$(κ^2-N,N-dpktah)Br] [25]. Our attempts to isolate *fac*-[Mn(CO)$_3$(κ^2-N,N-dpktsc)Br] from reaction of [Mn(CO)$_5$Br] with [dpktsc] in diethyl ether at different temperatures failed. When [Mn(CO)$_5$Br] was allowed to react with excess [dpktsc] in refluxing acetonitrile, [Mn(κ^3-N,N,S-dpktsc-H)$_2$]·2H_2O was isolated. In previous reports, [Mn(κ^3-N,N,S-dpktsc-H)$_2$] was prepared from reaction of [Mn(ClO_4)$_2$]·6H_2O with [dpktsc] in refluxing ethanol [17].

The identities of the isolated compounds were established from the results of their elemental analyses and spectroscopic properties. X-ray structural analyses confirmed the identities of [Mn(κ^4-N,N,S,N-dpktsc)Br]$_2$·$n$$CH_3CN$ ($n = 0$ or 1). The IR spectra of [Mn(κ^4-N,N,S,N-dpktsc)Br]$_2$ and [Mn(κ^3-N,N,S-dpktsc-H)$_2$]·2H_2O revealed peaks assignable to ν(N–H_2), ν(N–H), ν(C–H), combined ν(C=C) and ν(C=N) of the pyridine rings, and ν(C=S) vibrations and others consistent with the coordination of [dpktsc] to the manganese atom (see experimental section). The ν(C=S) stretching vibration of [Mn(κ^4-N,N,S,N-dpktsc)Br]$_2$ and [Mn(κ^3-N,N,S-dpktsc-H)$_2$]·2H_2O observed at 1225 and 1220 cm^{-1}, respectively, shifts to lower wavenumbers compared to ν(C=S) of [dpktsc] observed at 1242 cm^{-1}. This points to the weakening of the C=S bond due to coordination of the sulfur to the manganese. The ^{1}H NMR spectra of [Mn(κ^4-N,N,S,N-dpktsc)Br]$_2$ measured in DMSO-d_6 disclosed resonances consistent with the coordination of [dpktsc] to the metal. The chemical shifts of the protons of coordinated [dpktsc] in [Mn(κ^4-N,N,S,N-dpktsc)Br]$_2$ are similar to those of free [dpktsc] [22]. The resonances of [Mn(κ^4-N,N,S,N-dpktsc)Br]$_2$ are broader than those of free [dpktsc] due to the low solubility of [Mn(κ^4-N,N,S,N-dpktsc)Br]$_2$

Downloaded by [Institute Of Atmospheric Physics] at 15:25 09 December 2014

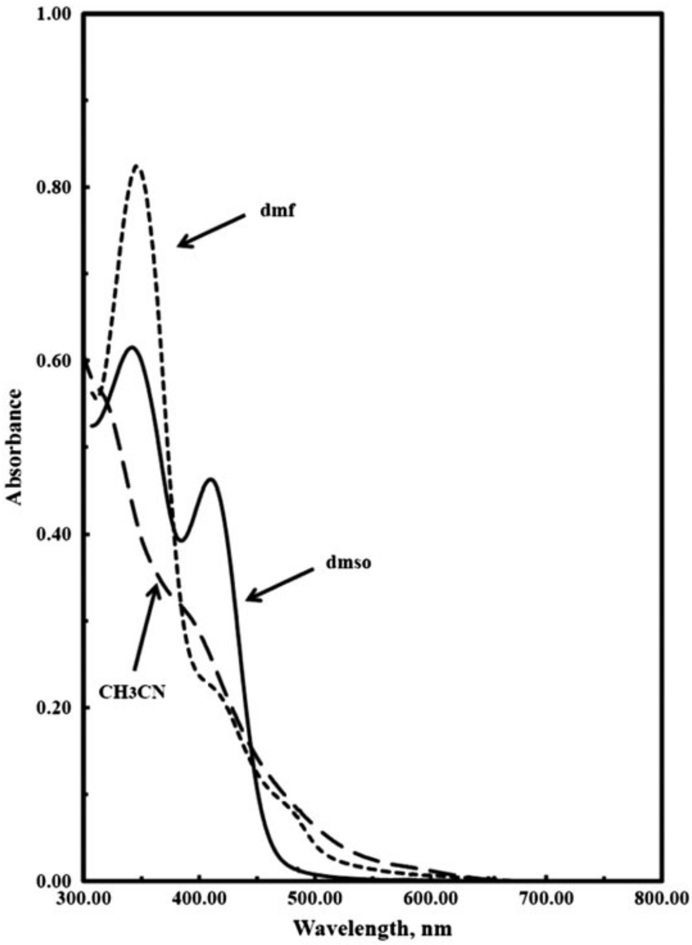

Figure 1. Electronic absorption of 2.5×10^{-5} M [Mn(κ^4-N,N,S,N-dpktsc)Br]$_2$ measured in DMF, DMSO and CH_3CN.

Downloaded by [Institute Of Atmospheric Physics] at 15:25 09 December 2014

in DMSO-d$_6$. The ^{1}H NMR spectrum of [Mn(κ^3-N,N,S-dpktsc-H)$_2$]·2H_2O measured in DMSO-d$_6$ revealed broad signals due to the paramagnetic character of Mn^{II}.

The electronic absorption spectra of [Mn(κ^4-N,N,S,N-dpktsc)Br]$_2$ measured in protophilic solvents (DMSO and DMF) are concentration dependent. Figure 1 shows the electronic absorption of [Mn(κ^4-N,N,S,N-dpktsc)Br]$_2$ in different solvents. In these spectra, two electronic transitions appeared. The electronic transitions in CH_3CN appeared at higher energy compared to those in protophilic solvents. In protophilic solvents, as the concentration of [Mn(κ^4-N,N,S,N-dpktsc)Br]$_2$ decreased, the ratio of the intensity of the high energy electronic transition, observed at ~345 nm, to the intensity of the low energy electronic transition observed at ~410 nm decreased. These results point to solvent–complex interaction. When excess benzoic acid was added to protophilic solutions of [Mn(κ^4-N,N,S,N-dpktsc) Br]$_2$, the intensity of the low energy electronic absorption disappeared and a significant increase in the intensity of the high energy electronic transition was observed. The opposite was observed when excess sodium benzoate was added to protophilic solutions of

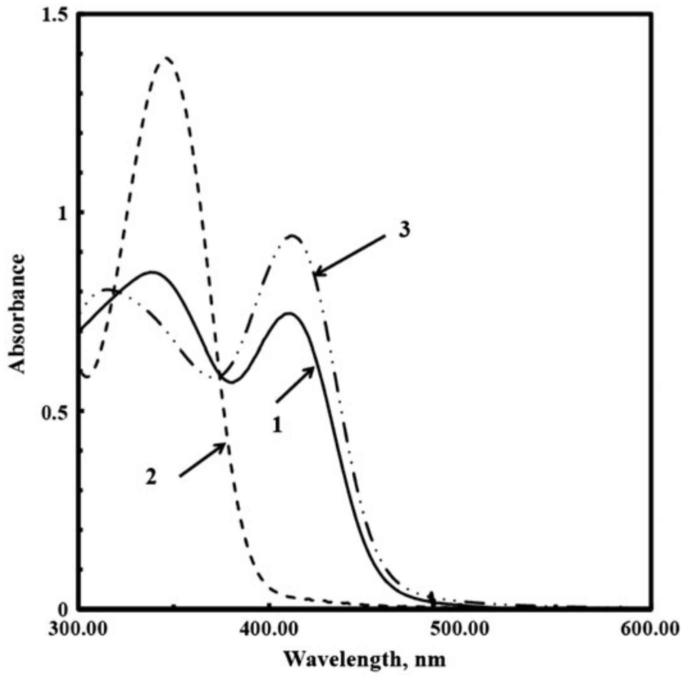

Figure 2. Electronic absorption spectra of 3.7×10^{-5} M DMSO solutions of [Mn(κ^4-N,N,S,N-dpktsc)Br]$_2$ measured in the absence and presence of excess benzoic acid and sodium benzoate.

[Mn(κ^4-N,N,S,N-dpktsc)Br]$_2$ (see figure 2). These results point to an acid–base inter-conversion between [Mn(κ^4-N,N,S,N-dpktsc)Br]$_2$ and its amide deprotonated conjugate base [Mn(κ^4-N,N,S,N-dpktsc-H)Br]$_2^-$ (see equations below). The ratio of the intensity of the low energy electronic transition to the intensity high energy electronic transition is significantly higher in DMSO compared to that in DMF (0.75 : 0.16) and hints to a stronger interaction between [Mn(κ^4-N,N,S,N-dpktsc)Br]$_2$ and DMSO compared to DMF. In the case of [Mn(κ^3-N,N,S-dpktsc-H)$_2$]·2H$_2$O, a single electronic transition appeared at ~410 nm in protophilic solvents. When excess benzoic acid was added to protophilic solutions of [Mn(κ^3-N,N,S-dpktsc-H)$_2$]·2H$_2$O, the electronic transition at ~410 nm disappeared and an electronic transition appeared at ~345 nm (see figure 3). The observed electronic transitions in [Mn(κ^4-N,N,S,N-dpktsc)Br]$_2$ and [Mn(κ^3-N,N,S-dpktsc-H)$_2$]·2H$_2$O are intra-ligand charge transfer transitions (ILCT) of the donor–acceptor type due to $n \rightarrow \pi^*$ and $\pi \rightarrow \pi^*$ of the thione moiety followed by thione to dpk charge transfer, mixed with metal-ligand charge transfer transitions. These transitions are similar to those reported for a variety of di-2-pyridyl ketone derivatives that include dpktsc and dpkhydrazones and their metal complexes [21–23, 26]. The high energy electronic transition is assigned to [Mn(κ^4-N,N,S,N-dpktsc)Br]$_2$ and [Mn(κ^3-N,N,S-dpktsc)$_2$]·2H$_2$O, and the low energy electronic transition is assigned to the amide deprotonated conjugated bases [Mn(κ^4-N,N,S,N-dpktsc-H)Br]$_2$ and [Mn(κ^3-N,N,S-dpktsc-H)$_2$]·2H$_2$O. In the spectra of protophilic solutions of [dpktsc], a shoulder appeared at ~400 nm and an intense absorption appeared at ~350 ± 5 nm [22]. The electronic absorption spectra of protophilic solutions of [dpktsc] are insensitive to bases and are highly sensitive to [MCl$_2$] (M = Zn, Cd, or Hg], i.e. [dpktsc] exhibits excellent chelating properties and sluggish acid–base inter-conversion [22].

Downloaded by [Institute Of Atmospheric Physics] at 15:25 09 December 2014

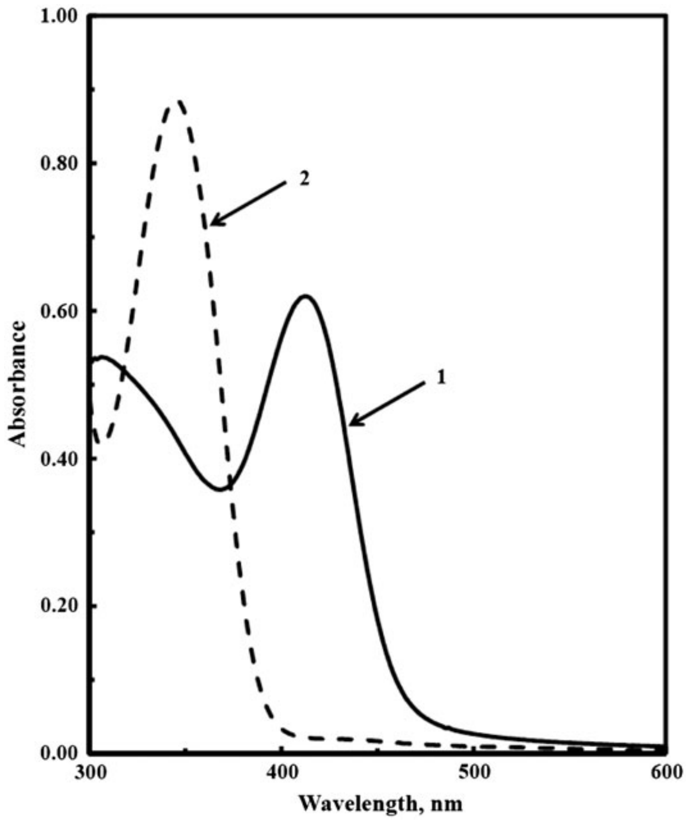

Figure 3. Electronic absorption spectra of 2.46×10^{-5} M DMSO solutions of [Mn(κ^3-N,N,S,-dpktsc-H)$_2$]·2H$_2$O measured in the absence (1) and presence of excess benzoic acid (2).

$$[\mathrm{Mn}(\kappa^4\text{-N, N, S, N-dpktsc})\mathrm{Br}]_2 + \mathrm{S} \rightleftarrows \{[\mathrm{Mn}(\kappa^4\text{-N, N, S, N-dpktsc-H})\mathrm{Br}]^-\}_2 + 2\mathrm{SH}^+ \quad (1)$$

$$[\mathrm{Mn}(\kappa^4\text{-N, N, S, N-dpktsc})\mathrm{Br}]_2 \underset{+\text{acid}}{\overset{\text{S+base}}{\rightleftarrows}} \{[\mathrm{Mn}(\kappa^4\text{-N, N, S, N-dpktsc-H})\mathrm{Br}]^-\}_2 \quad (2)$$

$$[\mathrm{Mn}(\kappa^3\text{-N, N, S-dpktsc-H})_2] \underset{+\text{base}}{\overset{\text{S+acid}}{\rightleftarrows}} [\mathrm{Mn}(\kappa^3\text{-N, N, S-dpktsc})_2] \quad (3)$$

$$(\mathrm{S} = \text{protophilic solvent})$$

The electrochemical properties of [Mn(κ^4-N,N,S,N-dpktsc)Br]$_2$ and [Mn(κ^3-N,N,S-dpktsc-H)$_2$]·2H$_2$O in DMF were investigated using voltammetric techniques (see figure 4). On a reductively initiated scan on [Mn(κ^4-N,N,S,N-dpktsc)Br]$_2$ (figure 4(a)), two closely spaced irreversible reductions due to $Mn^I \rightarrow Mn^0$ appeared at $E_{p,c} = -1.01$ and -1.07 V

Downloaded by [Institute Of Atmospheric Physics] at 15:25 09 December 2014

Downloaded by [Institute Of Atmospheric Physics] at 15:25 09 December 2014

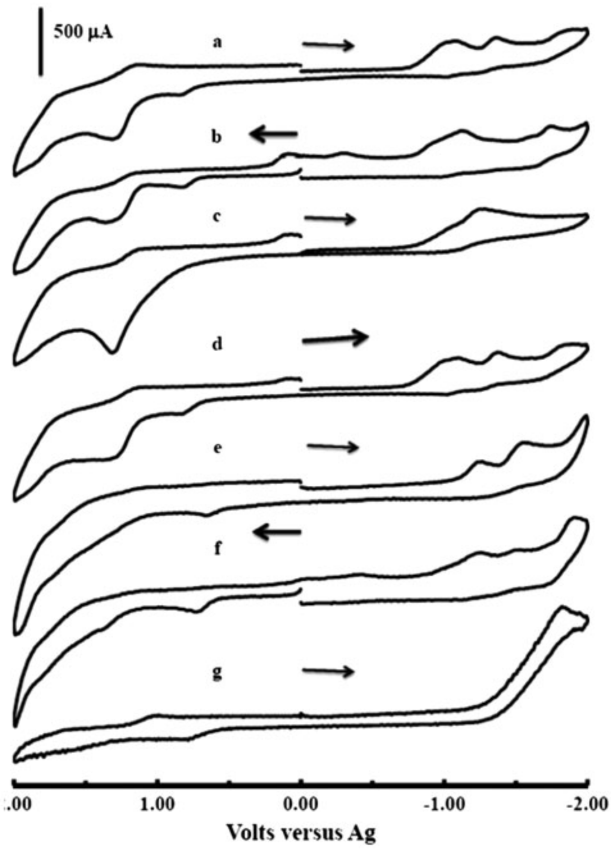

Figure 4. Cyclic voltammograms measured in DMF in the presence of 0.1 M in [N(n-Bu)$_4$](PF$_6$) at a glassy carbon working electrode at a scan rate of 400 mVs^{-1} *vs.* SCE. (a and b) [Mn(κ^4-N,N,S,N-dpktsc)Br]$_2$, (c) [Mn(κ^4-N,N,S,N-dpktsc)Br]$_2$ + CO_2, (d) [Mn(κ^4-N,N,S,N-dpktsc)Br]$_2$ + CO_2 + N_2, (e and f) [Mn(κ^3-N,N,S-dpktsc-H)$_2$]·2H_2O, (g) [Mn(κ^3-N,N,S-dpktsc-H)$_2$]·2H_2O + CO_2.

followed by two irreversible reductions at $E_{p,c} = -1.35$ and -1.90 V and two irreversible oxidations at $E_{p,a} = +0.84$ and +1.34 V. On an oxidatively initiated scan (figure 4(b)), an irreversible oxidation appeared at $E_{p,a} =$ +0.82 V, and two closely spaced oxidations due to $Mn^I \rightarrow Mn^{II}$ appeared at $E_{p,a} = +1.26$ and +1.38 V, respectively, followed by irreversible reductions at $E_{p,c} = +0.10$, −0.31, −0.94, −1.12, –1.61, and −1.73 V. The appearance of two closely spaced reductions and oxidations in these voltammograms is consistent with the dimeric nature of [Mn(κ^4-N,N,S,N-dpktsc)Br]$_2$ and are similar to the electrochemical signature of other previously reported dimers [36]. The irreversible oxidation at $E_{p,a} = \sim+0.82$ V is assigned to the 2Br^-/Br_2 oxidation. The other redox processes in these voltammograms are scanning direction dependent, hence electrochemically generated. Cyclic voltammograms of [Mn(κ^4-N,N,S,N-dpktsc)Br]$_2$ in the presence of CO_2 (figure 4(c)) show a pre-wave at $E_{p,c} = -1.02$ and irreversible reduction at $E_{p,c} = -1.25$ V and irreversible oxidation at $E_{p,a} =$ +1.30 V. When the electrochemical cell containing CO_2 was purged with N_2 (figure 4(d)), voltammatric signature similar to that obtained in the absence of CO_2 (figure 4(c)) was obtained on reductively initiated scan. These results show that the electrochemical reaction of CO_2 with [Mn(κ^4-N,N,S,N-dpktsc)Br]$_2$ led to the dissociation of the dimer. In the voltammograms of [Mn(κ^3-N,N,S-dpktsc-H)$_2$]·2H$_2$O, two well-separated irreversible reductions due to $Mn^{II} \rightarrow Mn^{I}$ and $Mn^{I} \rightarrow Mn^{0}$ appeared at $E_{p,c} = -1.22$ and -1.54 V plus other irreversible product waves. In the presence of CO_2, the first irreversible reduction wave disappeared and a significant increase in current appeared after the second reduction wave. An electrochemical signature similar to that in the absence of CO_2 was obtained when the cell containing CO_2 was purged with N_2. These results show that [Mn(κ^3-N,N, S-dpktsc-H)$_2$]·2H$_2$O is more electrochemically active toward CO_2 than [Mn(κ^4-N,N,S, N-dpktsc)Br]$_2$.

Views of the asymmetric units and molecular structures of [Mn(κ^4-N,N,S,N-dpktsc) Br]$_2$·nCH$_3$CN ($n = 0$ or 1) are shown in figures 5 and 6 and selected bond distances and angles are given in table 2. The molecular structures of the dimers reveal centrosymmetric

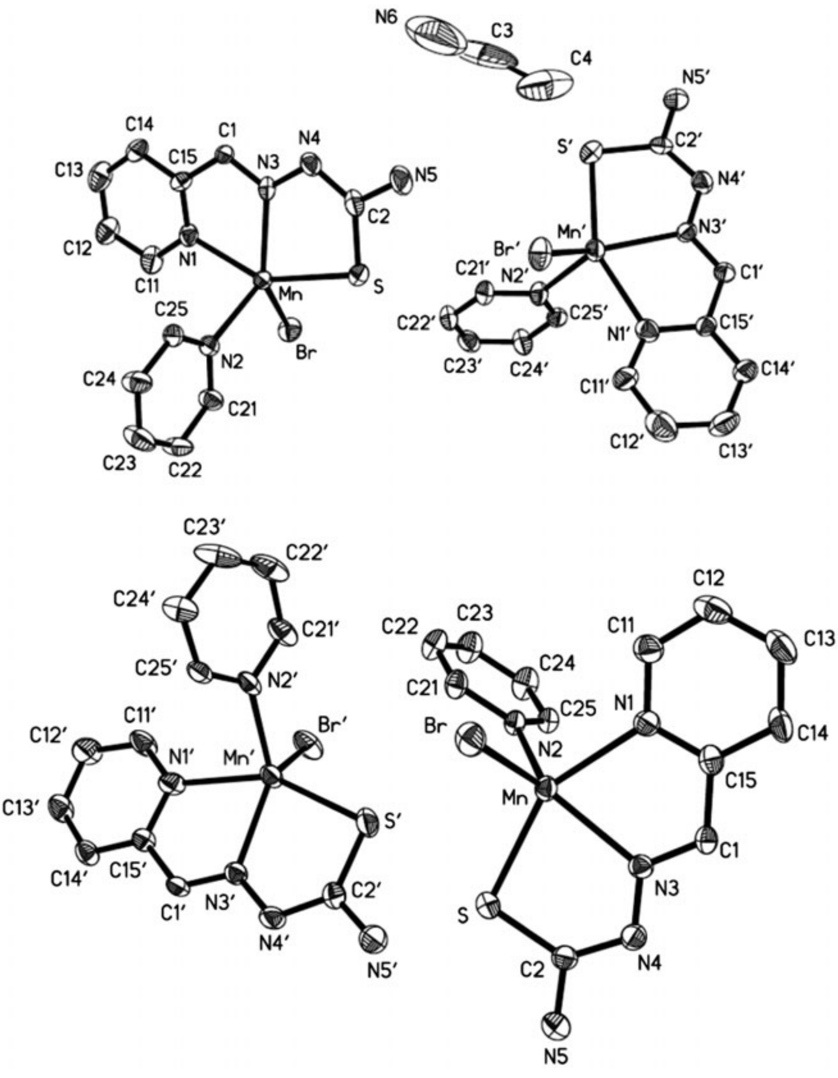

Figure 5. Views of the asymmetric units of [Mn(κ^4-N,N,S,N-dpktsc)Br]$_2$·nCH$_3$CN.

Downloaded by [Institute Of Atmospheric Physics] at 15:25 09 December 2014

Downloaded by [Institute Of Atmospheric Physics] at 15:25 09 December 2014

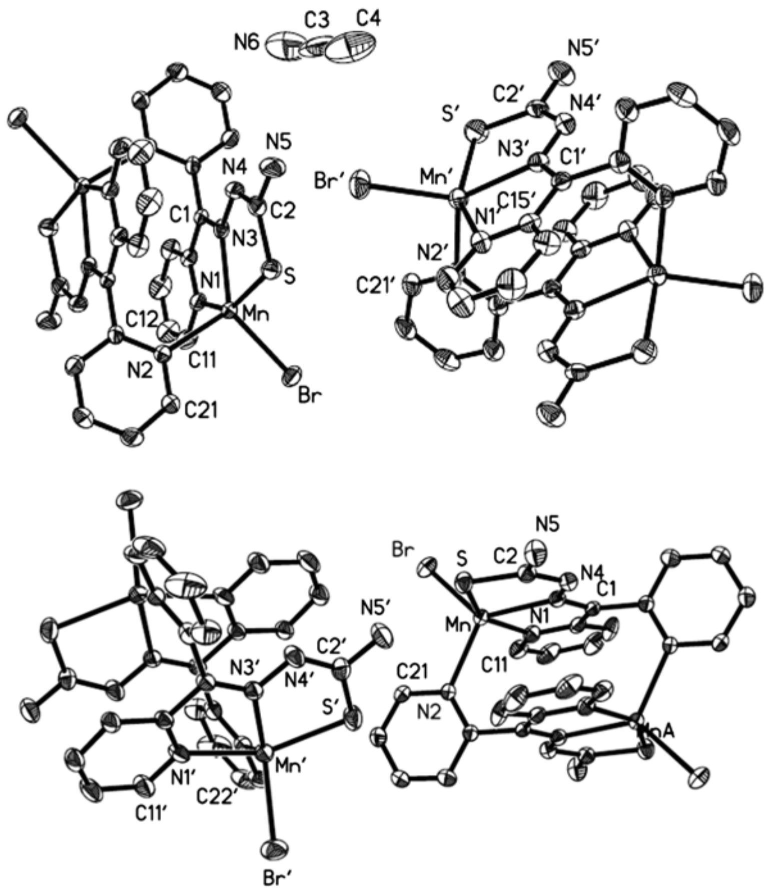

Figure 6. Views of the molecular structures of $[Mn(\kappa^4\text{-N,N,S,N-dpktsc})Br]_2 \cdot nCH_3CN$.

molecules. The unit cell of each dimer contains two independent $[Mn(\kappa^4$-N,N,S,N-dpktsc) $Br]_2$ units and one CH_3CN in the case of $n = 1$. The ligand [dpktsc] bridges two manganese atoms, binding to one manganese atom through the nitrogen atom of a pyridine ring, an imino nitrogen atom, and a sulfur atom of the thiosemicarbazone moiety, and coordinates to the other manganese atom through the nitrogen atom of the second pyridine ring. A bromine atom coordinates to each manganese atom in the dimer. The bond distances of coordinated atoms are normal and similar to those reported for other manganese compounds of di-2-pyridyl ketone derivatives, slightly longer (~0.1–0.3 Å) than those reported for copper compounds of di-2-pyridyl ketone thiosemicarbazone derivatives. The C-S bond distance (~1.73 Å) of coordinated [dpktsc] is close to a single C–S bond distance (~1.75 Å) reported in the literature [18]. The Mn-S bond distances (~2.45 Å) are of the same order as that reported for other related rhenium compounds (~2.50 Å) and significantly longer that those reported for Cu–S bond (~2.26 Å) in dimeric copper compounds of [dpktsc] [18, 19]. The Mn–N bonds of the chelating and bridging nitrogen atoms are of similar order, pointing to the absence of elongation of the bridging Mn–N ligand compared to the equatorial bonds. This is in contrast to the significant differences noted between the axial and

Table 2. Bond lengths [Å] and angles [°] for [Mn(κ[4]-N,N,S,N-dpktsc)Br]$_2$·nCH$_3$CN (n = 0 or 1).

	[Mn(κ[4]-N,N,S,N-dpktsc)Br]$_2$·CH$_3$CN	[Mn(κ[4]-N,N,S,N-dpktsc)Br]$_2$
Mn–N(1)	2.214(7)	2.210(4)
Mn–N(2)	2.230(7)	2.241(4)
Mn–N(3)	2.237(7)	2.249(3)
Mn–S	2.472(2)	2.4621(14)
Mn–Br	2.5076(13)	2.4967(8)
Mn′–N(2′)	2.219(7)	2.223(5)
Mn′–N(3′)	2.239(6)	2.235(4)
Mn′–N(1′)	2.247(8)	2.236(4)
Mn′–S′	2.456(3)	2.4571(15)
Mn′–Br′	2.5319(17)	2.5181(10)
S–C(2)	1.734(9)	1.735(4)
S′–C(2′)	1.720(8)	1.704(6)
N(3)–C(1)	1.301(10)	1.295(6)
N(3)–N(4)	1.360(8)	1.353(5)
N(4)–C(2)	1.343(12)	1.340(6)
N(5)–C(2)	1.332(10)	1.339(6)
N(3′)–C(1′)	1.288(10)	1.270(6)
N(3′)–N(4′)	1.383(10)	1.377(5)
N(1)–Mn–N(2)	94.5(2)	92.93(14)
N(1)–Mn–N(3)	72.3(2)	72.90(13)
N(2)–Mn–N(3)	119.3(2)	125.24(14)
N(1)–Mn–S	148.15(18)	149.61(10)
N(2)–Mn–S	105.86(19)	106.58(10)
N(3)–Mn–S	76.41(15)	76.81(10)
N(1)–Mn–Br	98.57(16)	96.63(10)
N(2)–Mn–Br	103.65(16)	105.03(10)
N(3)–Mn–Br	136.39(16)	128.61(10)
S–Mn–Br	99.99(6)	100.35(4)
τ	0.20	0.35
N(2′)–Mn′–N(3′)	121.2(2)	126.04(16)
N(2′)–Mn′–N(1′)	94.2(3)	90.29(15)
N(3′)–Mn′–N(1′)	72.8(2)	72.37(14)
N(2′)–Mn′–S′	103.4(2)	106.96(11)
N(3′)–Mn′–S′	77.19(19)	77.96(10)
N(1′)–Mn′–S′	149.93(18)	150.33(11)
N(2′)–Mn′–Br′	104.88(17)	104.65(11)
N(3′)–Mn′–Br′	131.71(16)	126.58(11)
N(1′)–Mn′–Br′	91.57(17)	93.71(12)
S′–Mn′–Br′	106.91(8)	104.58(6)
τ	0.30	0.40
C(2)–S–Mn	98.2(3)	98.22(16)
C(2′)–S′–Mn′	98.4(3)	97.66(17)
C(15)–N(1)–C(11)	119.3(7)	118.5(4)
C(15)–N(1)–Mn	117.5(5)	116.9(3)
C(11)–N(1)–Mn	123.2(6)	124.5(3)
C(25)–N(2)–C(21)	119.1(7)	118.3(3)
C(25)–N(2)–Mn	125.0(5)	125.4(3)
C(21)–N(2)–Mn	116.0(5)	116.3(3)
C(1)–N(3)–N(4)	116.3(6)	118.7(4)
C(1)–N(3)–Mn	118.5(5)	117.0(3)
N(4)–N(3)–Mn	125.1(5)	124.0(3)
C(2)–N(4)–N(3)	112.4(6)	113.3(4)
C(21′)–N(2′)–Mn′	117.7(6)	118.0(4)
C(25′)–N(2′)–Mn′	124.3(5)	125.4(3)
C(1′)–N(3′)–N(4′)	120.1(6)	118.1(4)
C(1′)–N(3′)–Mn′	117.4(5)	118.4(3)
N(4′)–N(3′)–Mn′	122.4(5)	123.0(3)

Symmetry transformations used to generate equivalent atoms: #1 $-x+2$, $-y+1$, $-z+1$; #2 $-x$, $-y+2$, $-z+2$.

Downloaded by [Institute Of Atmospheric Physics] at 15:25 09 December 2014

Downloaded by [Institute Of Atmospheric Physics] at 15:25 09 December 2014

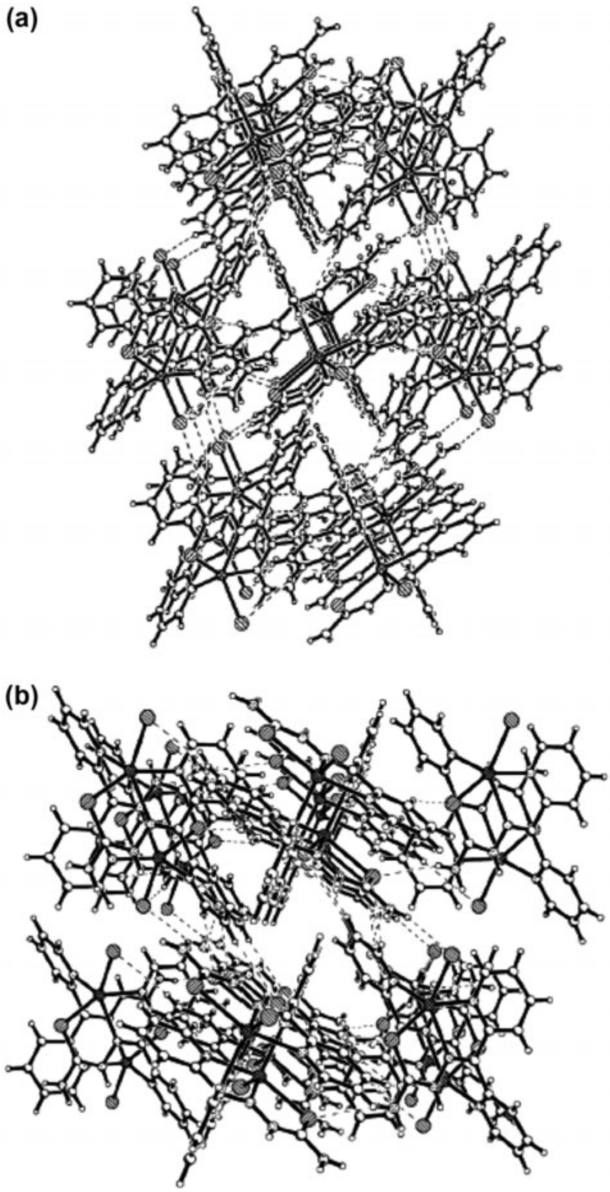

Figure 7. Views of the extended structures of [Mn(κ^4-N,N,S,N-dpktsc)Br]$_2$·CH_3CN (a) and [Mn(κ^4-N,N,S,N-dpktsc)Br]$_2$ (b).

equatorial Cu–N bonds reported for Cu-dpktsc dimers [18]. The trigonality indices (τ)[†] of the dimers in each unit cell show slight variations due to crystal packing. The coordination about each manganese atom is pseudo-square pyramidal and is similar to those reported for Cu-dpktsc dimers. The trigonality indices of the solvated dimers in the unit cell are smaller

[†]The trigonality index $(T) = (\beta - \alpha)/60$ with α and β are the two largest coordinated angles. $T = 0$ for an ideal square-pyramid ($\alpha = \beta = 180°$) and $T = 1$ for an ideal trigonal-bipyramid ($\alpha = 120°$ and $\beta = 180°$) [37].

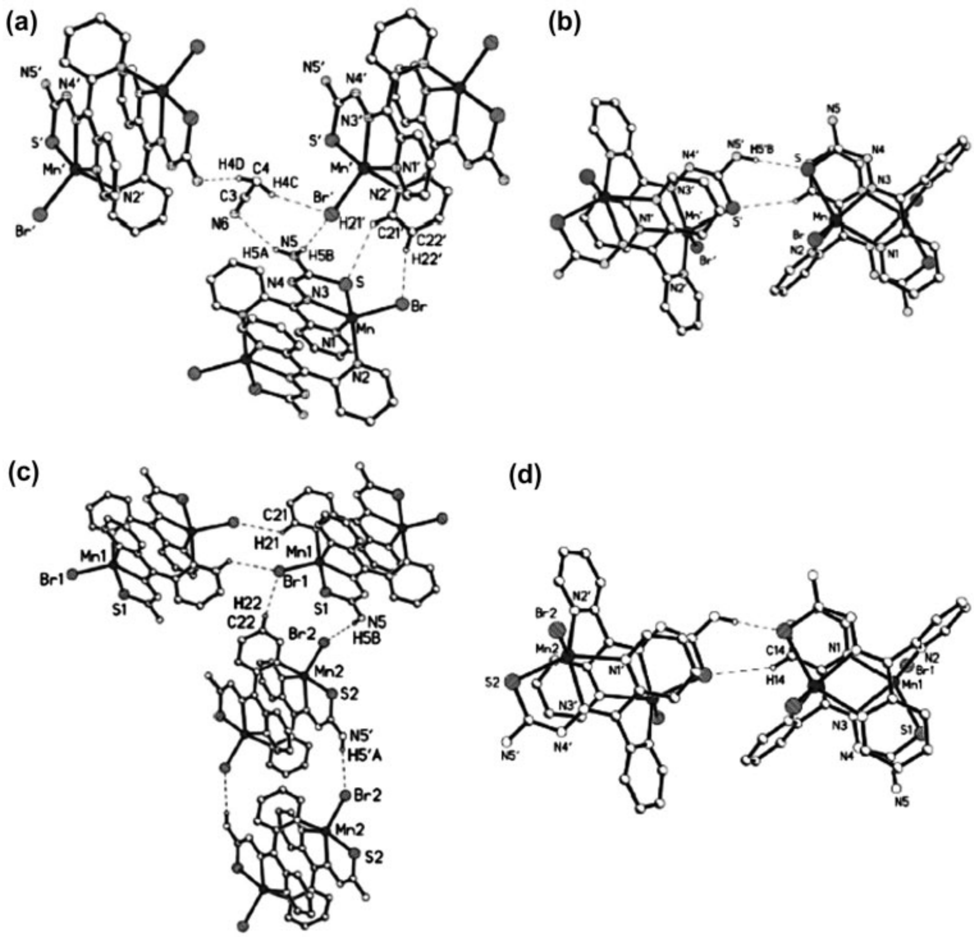

Figure 8. Views of the hydrogen bonds in [Mn(κ^4-N,N,S,N-dpktsc)Br]$_2$·CH$_3$CN (a and b) and [Mn(κ^4-N,N,S,N-dpktsc)Br]$_2$ (c and d).

Downloaded by [Institute Of Atmospheric Physics] at 15:25 09 December 2014

than those of solvent free dimers; thus, the coordination about the manganese atoms in [Mn(κ^4-N,N,S,N-dpktsc)Br]$_2$·CH$_3$CN is more close to square pyramidal than that of [Mn(κ^4-N,N,S,N-dpktsc)Br]$_2$.

Views of the extended structures of [Mn(κ^4-N,N,S,N-dpktsc)Br]$_2$·nCH$_3$CN ($n = 0$ or 1) are shown in figure 7 and reveal stacking of [Mn(κ^4-N,N,S,N-dpktsc)Br]$_2$·nCH$_3$CN ($n = 0$ or 1) locked via a network of non-covalent interactions and intermolecular voids. The structures of [Mn(κ^4-N,N,S,N-dpktsc)Br]$_2$·nCH$_3$CN ($n = 0$ or 1) are stabilized by an extensive network of hydrogen bonds (see figure 8 and table 3). The inter-planar distances between the chelating rings of 3.363 and 3.338 Å (solvated) and 3.328 and 3.348 Å (solvent free) show significant π-interactions between the chelating rings. Calculations of the solvent accessible volumes in [Mn(κ^4-N,N,S,N-dpktsc)Br]$_2$·nCH$_3$CN ($n = 0$ or 1) yielded 31.3 and 103.8 Å^3 of empty space in [Mn(κ^4-N,N,S,N-dpktsc)Br]$_2$·CH$_3$CN and [Mn(κ^4-N,N,S,N-dpktsc)Br]$_2$, respectively [35]. The vacant sites may arise from geometrical packing constraints and are due to loss of solvent of crystallization without structural collapse.

Table 3. Hydrogen bonds for [Mn(κ^4-N,N,S,N-dpktsc)Br]$_2$·nCH$_3$CN [Å and °].

D–H···A	d(D–H)	d(H···A)	d(D···A)	∠ (DHA)
[Mn(κ^4-N,N,S,N-dpktsc)Br]$_2$·CH$_3$CN				
N(5)–H(5A)···N(6)	0.86	2.459	3.275(3)	158.61
N(5)–H(5B)···Br′	0.86	2.634	3.473(3)	165.45
N(5′)–H(5’A)···Br′^{1}	0.86	3.083	3.675(3)	127.96
N(5)–H(5B)···S^2	0.86	2.675	3.440(3)	165.45
N(5′)–H(5’A)···C(12′)^2	0.86	3.46	3.524(16)	87.3
C(21′)–H(21′)···S	0.93	2.57	3.660(8)	122.4
C(21)–H(21)···S′	0.93	2.942	3.660(8)	135.1
C(4)–H(4D)···N5′	0.96	2.366	3.31(2)	167.7
C(14)–H(14)···S^3	0.93	2.82	3.543(8)	151.5
C(22)–H(22)….Br^4	0.93	3.037	3.768(9)	165.3
[Mn(κ^4-N,N,S,N-dpktsc)Br]$_2$				
N(5)–H(5B)···Br′	0.86	2.747	3.573(3)	161.56
N(5′)–H(5′A)···Br′^{5}	0.86	2.830	3.530(3)	139.73
N(5′)–H(5′B)···S	0.86	2.841	3.467(3)	131.04
C(21)–H(21)···Br^6	0.93	2.942	3.601(5)	129.1
C(22)–H(22)···Br^6	0.93	2.955	3.654(6)	173.7

Symmetry transformations used to generate equivalent atoms: $^1x-1, y, z$; $^2x-1, y, z$; $^32-x, 1-y, 1-z$; $^42-x, 2-y, 1-z$; $^51+x, y, z$, $^5x, y+1, z$; $^61-x, -y, 1-z$.

Due to their rich physico-chemical properties and potential applications in several areas, studies are in progress in our laboratory to explore the coordination chemistry of a variety of di-2-pyridyl ketone derivatives.

4. Conclusion

Reactions of [Mn(CO)$_5$Br] with [dpktsc] in CH$_3$CN gave the first manganese dimers of [dpktsc], [Mn(κ^4-N,N,S,N-dpktsc)Br]$_2$·nCH$_3$CN, along with mononuclear, [Mn(κ^3-N,N,S-dpktsc-H)$_2$]·2H$_2$O. The solid-state structure of [Mn(κ^4-N,N,S,N-dpktsc)Br]$_2$·nCH$_3$CN is stabilized by extensive network of non-covalent interactions. Spectroscopic measurements revealed sensitivity of [Mn(κ^4-N,N,S,N-dpktsc)Br]$_2$ and [Mn(κ^3-N,N,S-dpktsc-H)$_2$]·2H$_2$O to changes in their surroundings. [Mn(κ^3-N,N,S,-dpktsc-H)$_2$]·2H$_2$O is more electro-active toward CO_2 than [Mn(κ^4-N,N,S,N-dpktsc)Br]$_2$.

Acknowledgements

The authors acknowledge the University of the West Indies for financial support and Dr Marvadeen Singh-Wilmot for assistance with the solid-state structure of the solvated dimer.

References

[1] A. Garoufis, S.K. Hadjikakou, N. Hadjiliadis. *Coord. Chem. Rev.*, **253**, 1384 (2009).
[2] J.R. Dilworth, R. Hueting. *Inorg. Chim. Acta*, **389**, 3 (2012).
[3] D. Dayal, D. Palanimuthu, S.V. Shinde, K. Somasundaram, A.G. Samuelson. *J. Biol. Inorg. Chem.*, **16**, 621 (2011).
[4] J. Tian, D.M. Peehl, W. Zheng, S.J. Knox. *Cancer Lett.*, **298**, 231 (2010).

Downloaded by [Institute Of Atmospheric Physics] at 15:25 09 December 2014

[5] G. Pelosi, F. Bisceglie, F. Bignami, P. Ronzi, P. Schiavone, M.C. Re, C. Casoli, E. Pilotti. *J. Med. Chem.*, **53**, 8765 (2010).
[6] P. Paul, P. Sengupta, S. Bhattacharya. *J. Organomet. Chem.*, **724**, 281 (2013).
[7] D. Pandiarajan, R. Ramesh, Y. Liu, R. Suresh. *Inorg. Chem. Commun.*, **33**, 33 (2013).
[8] N.S. Youssef, A.M.A. El-Seidy, M. Schiavoni, B. Castano, F. Ragaini, E. Gallo, A. Caselli. *J. Organomet. Chem.*, **714**, 94 (2012).
[9] H. Yan, P. Chellan, T. Li, J. Mao, K. Chibale, G.S. Smith. *Tetrahedron Lett.*, **54**, 154 (2013).
[10] S.L. Ashok Kumar, M. Saravana Kumar, P.B. Sreeja, A. Sreekanth. *Spectrochim. Acta, Part A*, **113**, 123 (2013).
[11] S. Mandal, R. Modak, S. Goswami. *J. Mol. Struct.*, **1037**, 352 (2013).
[12] Z.-H. Xu, X.-F. Hou, W.-L. Xu, R. Guo, T.-C. Xiang. *Inorg. Chem. Commun.*, **34**, 42 (2013).
[13] Q. Lin, P. Chen, J. Liu, Y.-P. Fu, Y.-M. Zhang, T.-B. Wei. *Dyes Pigm.*, **98**, 100 (2013).
[14] C. Stefani, P.J. Jansson, E. Gutierrez, P.V. Bernhardt, D.R. Richardson, D.S. Kalinowski. *J. Med. Chem.*, **56**, 357 (2013).
[15] A.N. Kate, A.A. Kumbhar, A.V. Sapre, S.R. Peerannawar, S.P. Gejji. *J. Phys. Chem. A*, **117**, 5447 (2013).
[16] P.V. Bernhardt, P.C. Sharpe, M. Islam, D.B. Lovejoy, D.S. Kalinowski, D.R. Richardson. *J. Med. Chem.*, **52**, 407 (2009).
[17] A. Sreekanth, S. Sivakumar, M.R. Prathapachandra Kurup. *J. Mol. Struct.*, **655**, 47 (2003).
[18] C.Y. Duan, B.M. Wu, T.C.W. Mak. *J. Chem. Soc., Dalton Trans.*, 3485 (1996).
[19] G. Pereiras-Gabián, E.M. Vázquez-López, U. Abram. *Z. Anorg. Allg. Chem.*, **630**, 1665 (2004).
[20] G. Pereiras-Gabián, E.M. Vázquez-López, H. Braband, U. Abram. *Inorg. Chem.*, **44**, 834 (2005).
[21] M. Bakir, O. Brown. *J. Mol. Struct.*, **930**, 65 (2009).
[22] M. Bakir, O. Brown. *J. Mol. Struct.*, **1006**, 402 (2011).
[23] M. Bakir, C. McDermot, T. Johnson. *J. Mol. Struct.*, **1040**, 221 (2013).
[24] M. Bakir. *Eur. J. Inorg. Chem.*, **481**, (2002).
[25] M. Bakir, O. Green, M. Wilmot-Singh. *J. Mol. Struct.*, **967**, 174 (2010).
[26] M. Bakir, R.R. Conry, O. Green, W.H. Mulder. *J. Coord. Chem.*, **61**, 3066 (2008).
[27] T.A. Reena, M.R.P. Kurup. *Spectrochim. Acta, Part A*, **76**, 322 (2010).
[28] H. Görner. *J. Photochem. Photobiol., A*, **208**, 141 (2009).
[29] H.-S. Wang, Y. Song. *Inorg. Chem. Commun.*, **35**, 86 (2013).
[30] K.B. Szpakolski, K. Latham, C.J. Rix, J.M. White. *Inorg. Chim. Acta*, **376**, 628 (2011).
[31] J.M. Myers, Q. Cheng, W.E. Antholine, B. Kalyanaraman, A. Filipovska, E.S.J. Arnér, C.R. Myers. *Free Radical Biol. Med.*, **60**, 183 (2013).
[32] J.C. Yalowich, X. Wuc, R. Zhang, R. Kanagasabai, M. Hornbaker, B.B. Hasinoff. *Biochem. Pharmacol.*, **84**, 52 (2012).
[33] Bruker-SHELXTL, *Software Version 5.1*. Bruker AXS, Inc., Madison, Wisconsin, USA (1997).
[34] G.M. Sheldrick. *SHELX97 and SHELXL97*, University of Göttingen, Germany (1997).
[35] A.L. Spek. *Acta Cryst.*, **D65**, 148 (2009).
[36] M. Bakir, R.A. Walton. *Polyhedron*, **6**, 1925 (1987).
[37] A.W. Addison, T.N. Rao, J. Reedijk, J. van Rijn, G.C. Verschoor. *J. Chem. Soc., Dalton Trans.*, 1349 (1984).

Downloaded by [Institute Of Atmospheric Physics] at 15:25 09 December 2014